

Supporting information: Squeeze-film effect on atomically thin resonators in the high-pressure limit

Robin J. Dolleman,^{1,2,3} Debadi Chakraborty,² Daniel R. Ladiges,^{2,4}
Herre S. J. van der Zant,¹ John E. Sader,² and Peter G. Steeneken^{1,5}

¹*Kavli Institute of Nanoscience, Delft University of Technology, Lorentzweg 1, 2628CJ, Delft, The Netherlands*

²*ARC Centre of Excellence in Exciton Science, School of Mathematics and Statistics,
The University of Melbourne, Victoria, 3010, Australia*

³*Present address: Second Institute of Physics, RWTH Aachen University, 52074, Aachen, Germany*

⁴*Center for Computational Sciences and Engineering,
Lawrence Berkeley National Laboratory, 1 Cyclotron Rd, Berkeley, CA 94720, USA*

⁵*Department of Precision and Microsystems Engineering,
Delft University of Technology, Mekelweg 2, 2628 CD, Delft, The Netherlands**

S1: Methods.

Fabrication of the samples starts on silicon dies with ~ 285 nm of silicon dioxide. Dumbbell-shaped cavities are etched in the silicon dioxide layer, with a total depth of approximately 300 nm. Single layer graphene grown by chemical vapor deposition was transferred on top of this substrate using a supporting polymer. This polymer is dissolved, and the sample is subsequently dried using CO₂ critical point drying. Besides removing the polymer, this process is used to break the weakest part of the dumbbell, leaving a suspended circular membrane with a venting channel to the environment on the other side (Figs. 1 a, c-e in the main text). The venting channel prevents that pressure differences across the membrane can alter the tension and resonance frequency of the membrane, and thus it ensures that any observed frequency shifts can be attributed to the squeeze-film effect.

Figure 1b in the main text shows the experimental setup to actuate and detect graphene's motion in a controlled gaseous environment. The sample is mounted in a vacuum chamber, which is carefully tested for leaks to ensure the gas composition inside the chamber. A voltage-controlled dual-valve pressure controller is used to control the pressure in this chamber. Eight different gases can be connected to the input of the controller to select the type of gas. A red helium-neon laser is used to read-out the membrane motion by Fabry-Perot interferometry [1, 2]. The silicon substrate acts as a fixed mirror, while the suspended graphene membrane acts as the moving mirror. A blue diode laser is used to actuate the motion of the membrane by opto-thermally heating the membrane, which will experience a force due to thermal expansion [3, 4]. A red laser power of 2 mW and a blue laser power of 0.3 mW was used, both powers are measured before the objective.

The squeeze-film effect is measured by characterizing the membrane's amplitude of motion as a function of the frequency of the opto-thermal actuation, which is repeated at different pressures set by the pressure controller. To correct for any frequency dependence arising from the electronic components in the setup, the response of the setup is measured when the blue laser is directly illuminating the photodetector. This measurement is then used to deconvolve the measured response, two examples of such corrected responses are shown in Figs. 1e and f in the main text. To fit a harmonic oscillator response to the data, we must consider the thermal delay, which causes the actuation force to become frequency dependent [3, 5, 6]. A further frequency dependence can emerge from gas leakage, which has an identical frequency dependence [7]. This frequency dependence is corrected by fitting the response with a single thermal time constant model:

$$x = \frac{A}{\omega^2\tau^2 + 1} - \frac{iA\omega\tau}{\omega^2\tau^2 + 1}, \quad (\text{S1})$$

where A is used as a fitting variable. We fit to the imaginary part of the data to extract A and τ ; and use those parameters to again deconvolve the data with Eq. S1. In these measurements, usually either thermal or gas leakage effects dominate the response, and a single relaxation time model provided a good fit. However, at some pressures both thermal and gas delay effects occur at the same time, and a single relaxation time does not provide a good fit. In those cases, no frequency and quality factor are fit, and those data points are omitted. After the correction for the frequency dependence of the actuation force, the data is fit using a simple harmonic oscillator model without an additional background. In the example traces in Figs. 1e and f in the main text, the fits to the harmonic oscillator are again multiplied with the fit to frequency-dependence of the actuation force at low frequencies. This shows that

the fitting procedure can accurately represent the resonance peak and the background. If the frequency dependence of the actuation force is not considered, the background will cause the fitting to underestimate the resonance frequency when the quality factor of the resonance is low.

S2: Additional measurements

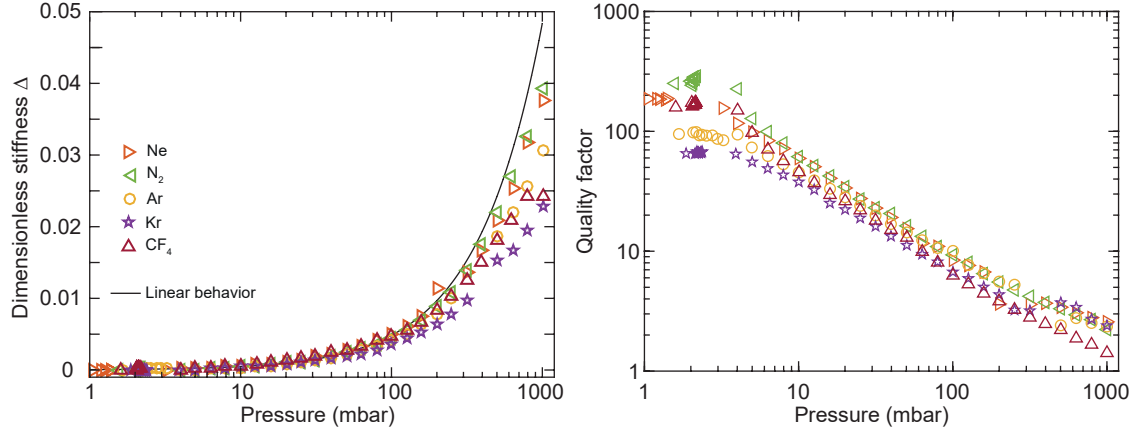


FIG. S1. Remainder of the dataset in Fig. 2 in the main text.

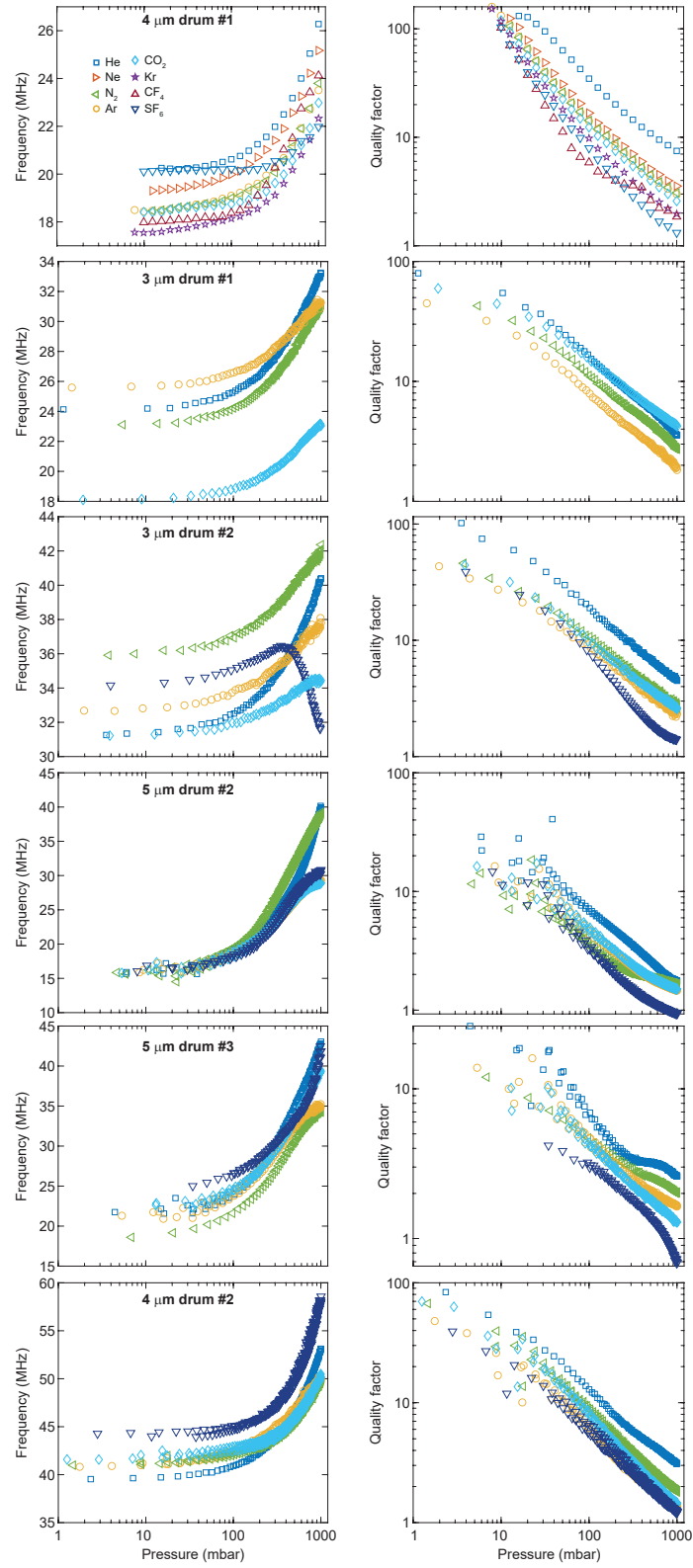


FIG. S2. Resonance frequency and Q-factor of 6 more samples not shown in the main text.

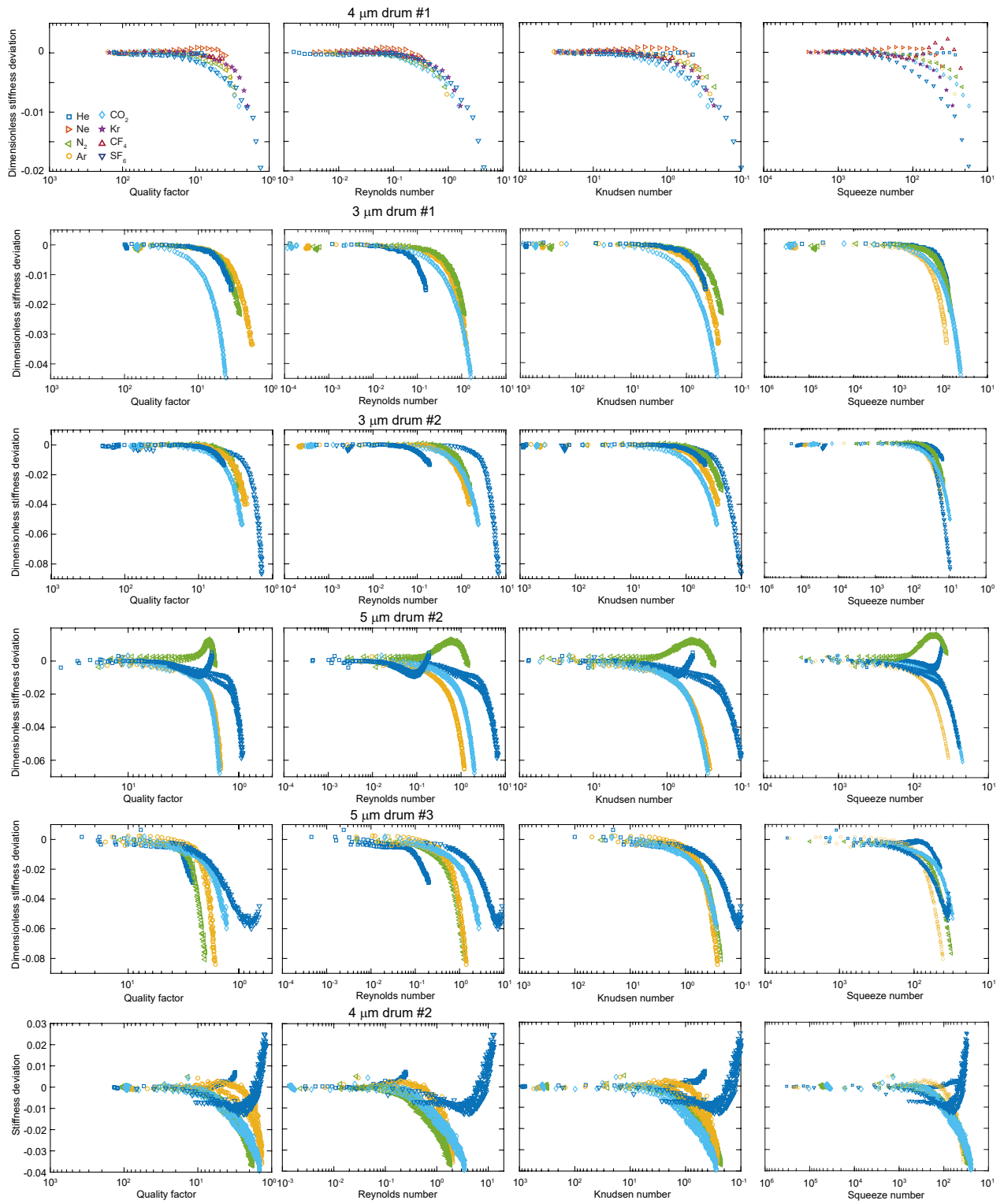


FIG. S3. Dimensionless stiffness deviation as a function of dimensionless parameters for 6 more samples not shown in the main text.

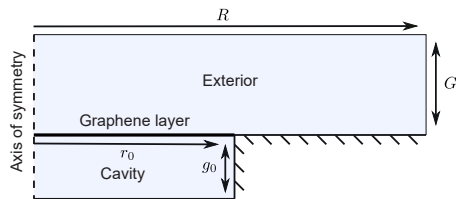


FIG. S4. Schematic of domain used for numerical simulations.

S3: Simulations

Figure S4 shows a schematic of the domain used in both numerical simulations. For both the continuum and Boltzmann Transport Equation (BTE) simulations the domain was taken to be axisymmetric around the center of the device. For each of the pressures shown in Fig. 6 in the main text, the bounds on the exterior domain, R and G , were increased until a consistent frequency and quality factor was achieved; bounds of at least $R = 3r_0$ and $G = 40g_0$ were used. While for the continuum simulation the drum was taken to be fully enclosed, for the BTE simulation the drum walls were taken to be slightly porous to simulate the presence of the venting channel, with the porosity set to match the proportion of the drum wall occupied by the channel; in the results shown here, this was set at 5%. As expected, varying this parameter had a negligible effect on the measured frequency.

As discussed in the main text, the continuum simulations applied the eigenfrequency solver of COMSOL [8, 9] to the compressible Stokes equation for the gas (with no-slip boundary conditions), and Navier's equation for the solid. The BTE simulations employed a custom code solving the frequency domain Boltzmann-BGK equation [10–12] for the gas, with diffuse boundary conditions [13]; this boundary condition naturally includes slip as the gas becomes rarefied. They were coupled with an axisymmetric membrane equation to represent the graphene. For both the continuum and BTE simulations the physical parameters of the graphene were inferred by matching to the frequency measured in a vacuum.

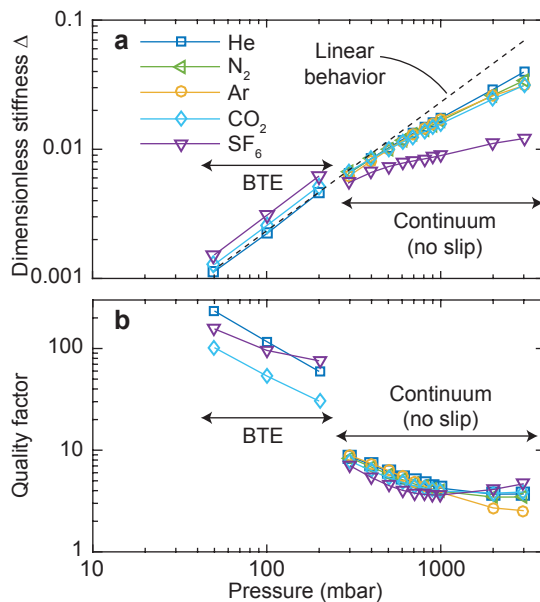


FIG. S5. Simulations of resonance frequency and quality factor for a representative squeeze-film pressure sensor. The simulations shown here are used to perform the analysis shown in the main text. **a** Dimensionless frequency shift, showing a clear deviation for sulphur hexafluoride. **b** Quality factor of resonance, showing the increase at high pressures discussed in the main text.

Figure S5 shows the dimensionless frequency shift and the quality factor from simulations of the previously published 31-layer device. In agreement with the experiments performed here, we find that the continuum simulations predict deviations from the linear stiffness increase as a function of pressure (Fig. S5a). Sulphur hexafluoride shows a clear deviation from the other gases. The simulated quality factor as a function of pressure in Fig. S5 shows a similar weak gas dependence as a function of molecular weight. At high pressures, however, the simulations suggest that the

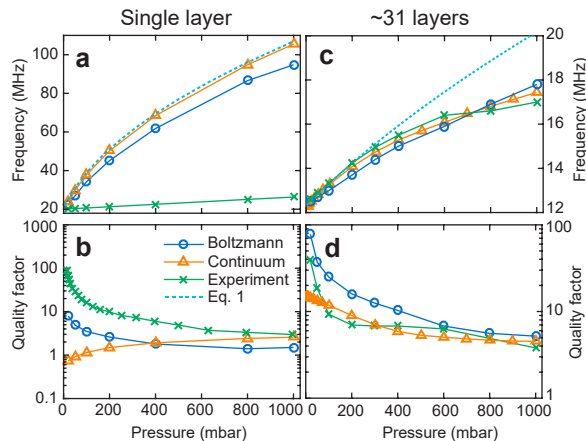


FIG. S6. **a** Continuum and Boltzmann simulations of the resonance frequency of a 4-micron diameter single-layer graphene drum in a helium environment as a function of pressure in the case of single-layer graphene, compared to Eq. 1 in the main text and experimental data. The simulations assume the theoretical mass of a clean single-layer graphene membrane. **b** Quality factor of resonance corresponding to figure **b**. **c** Resonance frequency in the case of a 5-micron diameter 31-layer graphene drum in a nitrogen environment and **d** quality factor of resonance.

quality factor could increase as a function of pressure. This behaviour has not been observed in experiments, possibly due to the limited pressure range that could be achieved, but is predicted by the single relaxation time model as discussed in the main text. The BTE simulations show a significantly larger quality factor since slip flow is included in this model. The model captures the pressure and gas-dependent trends of the quality factor that are observed in the experimental data but produces an upshift as function of pressure in the case of SF_6 that is not observed in the experiments.

Figure S6(a-b) shows additional simulation results for a 4-micron diameter single-layer graphene membrane in a helium environment, compared to experimental data. In these simulations we assume the single layer graphene has its theoretical mass of $7.7 \times 10^{-7} \text{ kg/m}^2$. In the experiments with single-layer graphene devices a much lower frequency shift is observed compared to the simulations, which may be attributed to additional mass on the single-layer graphene resonator which lowers the resonance frequency and squeeze-number (Fig. S6a). Even though the simulations suggest that the quality factor of the resonator will be much lower if the mass is reduced (Fig. S6b), the deviations in the resonance frequency are predicted to be small. This is possible because such a clean resonator will operate in the regime where $p_a/g_0\rho h$ is very large, which corresponds to the high-pressure lines in Fig. 5 in the main text. Figure S6(c-d) simulate the previously published 31-layer device [14] in a nitrogen environment. This serves as a benchmark for the simulations, but also shows that the deviations from Eq. 1 in the main text can be reproduced in the simulations if the mass of the membrane is increased.

S4: Relation between Q-factor and dimensionless number σ

To describe the graphene squeeze-film pressure sensor, we make a model with a single degree of freedom for the displacement x of the fundamental mode of the graphene membrane:

$$-\omega^2 x + i\omega \frac{2}{\tau_0} x + \omega_0^2 x = \beta \Delta p, \quad (\text{S2})$$

where ω is the radial frequency, τ_0 the exponential decay time of the membrane in vacuum, ω_0 is the resonance frequency, Δp the pressure difference over the membrane due to the squeeze-film effect, β is a proportionality constant. For the pressure in the cavity, we take a one-dimensional approximation by assuming the cavity has using a single relaxation time τ_g (which is the leak time):

$$i\omega \Delta p + \frac{1}{\tau_g} \Delta p = \gamma i\omega x, \quad (\text{S3})$$

where γ is another proportionality constant.

To find the free equation of motion we solve Eq. S3 for Δp :

$$\begin{aligned} (i\omega + \frac{1}{\tau_g})\Delta p &= \gamma i\omega x, \\ \Delta p &= \frac{i\omega\gamma}{i\omega + \frac{1}{\tau_g}} = \gamma \frac{i\omega\tau_g}{i\omega\tau_g + 1}, \\ \Delta p &= \gamma \frac{\omega^2\tau_g^2}{\omega^2\tau_g^2 + 1} + \gamma \frac{i\omega\tau_g}{\omega^2\tau_g^2 + 1}, \end{aligned} \quad (\text{S4})$$

This can be substituted into Eq. S2:

$$-\omega^2 x + i\omega \frac{2}{\tau_0} x + \omega_0^2 x = \beta\gamma \frac{\omega^2\tau_g^2}{\omega^2\tau_g^2 + 1} + \beta\gamma \frac{i\omega\tau_g}{\omega^2\tau_g^2 + 1}, \quad (\text{S5})$$

$$-\omega^2 x + i\omega \left(\frac{2}{\tau_0} - \beta\gamma \frac{\tau_g}{\omega^2\tau_g^2 + 1} \right) x + \left(\omega_0^2 - \beta\gamma \frac{\omega^2\tau_g^2}{\omega^2\tau_g^2 + 1} \right) x = 0, \quad (\text{S6})$$

By comparing the case $\omega\tau_g \gg 1$, we note that $\beta\gamma = -\frac{p_a}{g_0\rho h}$ where p_a is the atmospheric pressure, g_0 the gap size and ρh the membrane's mass per unit square. The stiffness of the system becomes:

$$\omega_f^2 = \omega_0^2 + \frac{p_a}{g_0\rho h} \frac{\omega^2\tau_g^2}{\omega^2\tau_g^2 + 1}. \quad (\text{S7})$$

The damping becomes:

$$\Gamma_f = \frac{2}{\tau_0} + \frac{p_a}{g_0\rho h} \frac{\tau_g}{\omega^2\tau_g^2 + 1}. \quad (\text{S8})$$

In the case where $\tau_0 \ll \tau_g$ and close to the resonance frequency:

$$\Gamma_f \approx \frac{p_a}{g_0\rho h} \frac{\tau_g}{\omega_f^2\tau_g^2 + 1}, \quad (\text{S9})$$

giving the equation of motion:

$$-\omega^2 x + \frac{p_a}{g_0\rho h} \frac{\omega_f\tau_g}{\omega_f^2\tau_g^2 + 1} x + \left(\omega_0^2 + \frac{p_a}{g_0\rho h} \frac{\omega_f^2\tau_g^2}{\omega_f^2\tau_g^2 + 1} \right) x = 0. \quad (\text{S10})$$

The dimensionless number σ compares the timescale of the compression to the timescale of the leakage:

$$\sigma = \tau_g\omega_f, \quad (\text{S11})$$

resulting in:

$$-\omega^2 x + i \frac{p_a}{g_0\rho h} \frac{\sigma}{\sigma^2 + 1} x + \left(\omega_0^2 + \frac{p_a}{g_0\rho h} \frac{\sigma^2}{\sigma^2 + 1} \right) x = 0, \quad (\text{S12})$$

The complex eigenvalues of this equation are given by:

$$\omega^2 = \omega_0^2 + \frac{p_a}{g_0\rho h} \frac{\sigma^2}{\sigma^2 + 1} + i \frac{p_a}{g_0\rho h} \frac{\sigma}{\sigma^2 + 1}, \quad (\text{S13})$$

$$\begin{aligned} \omega &= \sqrt[4]{\left(\frac{p_a}{g_0\rho h} \frac{\sigma(\sigma+1)}{\sigma^2+1} \right)^2 + \left(\frac{p_a}{g_0\rho h} \frac{\sigma}{\sigma^2+1} \right)^2} \times \\ &\cos\left(\frac{1}{2} \arg\left(\omega_0^2 + \frac{p_a}{g_0\rho h} \frac{\sigma^2}{\sigma^2+1} + i \frac{p_a}{g_0\rho h} \frac{\sigma}{\sigma^2+1} \right) \right) + \\ &i \sqrt[4]{\left(\frac{p_a}{g_0\rho h} \frac{\sigma(\sigma+1)}{\sigma^2+1} \right)^2 + \left(\frac{p_a}{g_0\rho h} \frac{\sigma}{\sigma^2+1} \right)^2} \times \\ &\sin\left(\frac{1}{2} \arg\left(\omega_0^2 + \frac{p_a}{g_0\rho h} \frac{\sigma^2}{\sigma^2+1} + i \frac{p_a}{g_0\rho h} \frac{\sigma}{\sigma^2+1} \right) \right). \end{aligned} \quad (\text{S14})$$

Using $Q_f = \mathcal{R}(\omega)/2\mathcal{I}(\omega)$:

$$\begin{aligned}
Q_f^2 &= \frac{\cos^2\left(\frac{1}{2}\arg\left(\omega_0^2 + \frac{p_a}{g_0\rho h}\frac{\sigma^2}{\sigma^2+1} + i\frac{p_a}{g_0\rho h}\frac{\sigma}{\sigma^2+1}\right)\right)}{4\sin^2\left(\frac{1}{2}\arg\left(\omega_0^2 + \frac{p_a}{g_0\rho h}\frac{\sigma^2}{\sigma^2+1} + i\frac{p_a}{g_0\rho h}\frac{\sigma}{\sigma^2+1}\right)\right)} \\
Q_f &= \frac{1}{2}\cot\left(\frac{1}{2}\arctan\left(\frac{\frac{p_a}{g_0\rho h}\frac{\sigma}{\sigma^2+1}}{\omega_0^2 + \frac{p_a}{g_0\rho h}\frac{\sigma^2}{\sigma^2+1}}\right)\right) \\
Q_f &= \frac{1}{2}\cot\left(\frac{1}{2}\arctan\left(\frac{\frac{\sigma}{\sigma^2+1}}{\frac{\omega_0^2}{\omega_{sqz}^2} + \frac{\sigma^2}{\sigma^2+1}}\right)\right),
\end{aligned} \tag{S15}$$

$$Q_f = \frac{\sqrt{\xi^2 + 1} + 1}{2\xi}, \tag{S16}$$

where:

$$\xi = \frac{\sigma}{\frac{\omega_0^2}{\omega_{sqz}^2}(\sigma^2 + 1) + \sigma^2}. \tag{S17}$$

S5: RELATION BETWEEN RELATIVE STIFFNESS DEVIATION AND Q FACTOR

In the main text, we define the relative stiffness deviation as:

$$\Delta_{\text{rel}} = \frac{\Delta - \Delta_{\text{lin}}}{\Delta_{\text{lin}}} \tag{S18}$$

To calculate this, we need the resonance frequency, which is given by the absolute value of ω in Eq. 7 in the main text:

$$|\omega| = \sqrt[4]{\frac{\omega_0^4 + \sigma^2\left(\omega_0^2 + \frac{p_a}{g_0\rho h}\right)^2}{\sigma^2 + 1}} \tag{S19}$$

If we assume Δ_{lin} is perfectly described by Eq. 1 from the main text, and that Δ is given by the real part of Eq. 7, we obtain:

$$\Delta_{\text{rel}} = \frac{g_0\rho h}{p_a} \sqrt{\frac{\omega_0^4 + \sigma^2\left(\omega_0^2 + \frac{p_a}{g_0\rho h}\right)^2}{\sigma^2 + 1}} - \frac{\omega_0^2 g_0\rho h}{p_a} - 1 \tag{S20}$$

Note, that by using Δ_{rel} , instead of $\Delta - \Delta_{\text{lin}}$, the theoretical value of ρh and p_{ref} used for the normalization in Eq. 2 in the main text have dropped out. Δ_{rel} now only depends on the real pressure and mass of the device. Next, we invert this equation to obtain an expression for σ , keeping only the positive solution:

$$\sigma = \frac{i\sqrt{\Delta_{\text{rel}} + 1}\sqrt{2\omega_0^2 + \frac{p_a}{g_0\rho h}\Delta_{\text{rel}} + \frac{p_a}{g_0\rho h}}}{\sqrt{\Delta_{\text{rel}}}\sqrt{2\omega_0^2 + \frac{p_a}{g_0\rho h}\Delta_{\text{rel}} + 2\frac{p_a}{g_0\rho h}}} \tag{S21}$$

This can then be evaluated at different values of Δ_{rel} and substituted into Eqs. S16–S17 to produce the red lines in Fig. 5 in the main text.

S6: COMPARISON BETWEEN LINEAR SLOPES

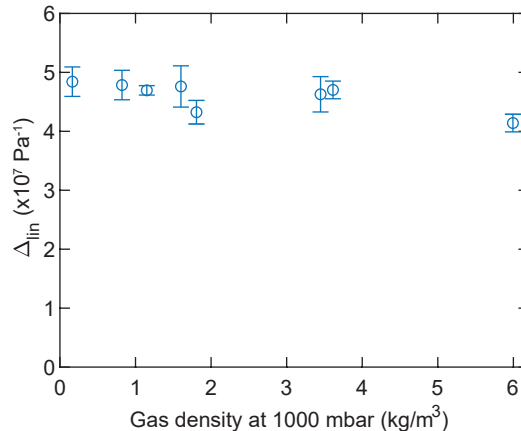


FIG. S7. Comparison of the slope of the linear stiffness (Δ_{lin}) as a function of density of the different gases for 5-micron diameter drum nr. 1. This shows that the compression of the gas is well-approximated as isothermal, since a strong gas dependence is expected for adiabatic compression [15]. Furthermore, this shows that the change in resonance frequency can be attributed to the squeeze-film effect, and that effects from mass loading on the top of the membrane are small.

* P.G.Steeneken@tudelft.nl

- [1] Andres Castellanos-Gomez, Ronald van Leeuwen, Michele Buscema, Herre SJ van der Zant, Gary A Steele, and Warner J Venstra, “Single-layer MoS₂ mechanical resonators,” *Advanced Materials* **25**, 6719–6723 (2013).
- [2] Robin J Dolleman, Dejan Davidovikj, Herre SJ van der Zant, and Peter G Steeneken, “Amplitude calibration of 2D mechanical resonators by nonlinear optical transduction,” *Applied Physics Letters* **111**, 253104 (2017).
- [3] Robin J Dolleman, Samer Hourri, Dejan Davidovikj, Santiago J Cartamil-Bueno, Yaroslav M Blanter, Herre SJ van der Zant, and Peter G Steeneken, “Optomechanics for thermal characterization of suspended graphene,” *Physical Review B* **96**, 165421 (2017).
- [4] Robin J Dolleman, Samer Hourri, Abhilash Chandrashekar, Farbod Alijani, Herre SJ van der Zant, and Peter G Steeneken, “Opto-thermally excited multimode parametric resonance in graphene membranes,” *Scientific Reports* **8**, 9366 (2018).
- [5] Robin J Dolleman, David Lloyd, Martin Lee, J Scott Bunch, Herre SJ van der Zant, and Peter G Steeneken, “Transient thermal characterization of suspended monolayer MoS₂,” *Physical Review Materials* **2**, 114008 (2018).
- [6] Robin J Dolleman, Gerard J Verbiest, Yaroslav M Blanter, Herre SJ van der Zant, and Peter G Steeneken, “Nonequilibrium thermodynamics of acoustic phonons in suspended graphene,” *Physical Review Research* **2**, 012058 (2020).
- [7] IE Rosłoń, RJ Dolleman, H Licona, M Lee, M Šiškins, H Lebius, L Madauś, M Schleberger, F Alijani, HSJ van der Zant, and PG Steeneken, “High-frequency gas effusion through nanopores in suspended graphene,” *Nature Communications* **11**, 6025 (2020).
- [8] Debadi Chakraborty, Emma van Leeuwen, Matthew Pelton, and John E. Sader, “Vibration of nanoparticles in viscous fluids,” *The Journal of Physical Chemistry C* **117**, 8536–8544 (2013).
- [9] Debadi Chakraborty and John E. Sader, “Constitutive models for linear compressible viscoelastic flows of simple liquids at nanometer length scales,” *Physics of Fluids* **27**, 052002 (2015).
- [10] Daniel R Ladiges and John E Sader, “Frequency-domain Monte Carlo method for linear oscillatory gas flows,” *Journal of Computational Physics* **284**, 351–366 (2015).
- [11] Daniel R Ladiges and John E Sader, “Frequency-domain deviational Monte Carlo method for linear oscillatory gas flows,” *Physics of Fluids* **27**, 102002 (2015).
- [12] Prabhu Lal Bhatnagar, Eugene P Gross, and Max Krook, “A model for collision processes in gases. I. small amplitude processes in charged and neutral one-component systems,” *Physical Review* **94**, 511 (1954).
- [13] G.A. Bird, *Molecular Gas Dynamics and the Direct Simulation of Gas Flows*, Vol. 1 (Oxford University Press, Oxford, Great Britain, 1994).
- [14] Robin Joey Dolleman, Dejan Davidovikj, Santiago José Cartamil-Bueno, Herre SJ van der Zant, and Peter Gerard Steeneken, “Graphene squeeze-film pressure sensors,” *Nano Letters* **16**, 568–571 (2016).
- [15] M Andrews, I Harris, and G Turner, “A comparison of squeeze-film theory with measurements on a microstructure,” *Sensors and Actuators A: Physical* **36**, 79–87 (1993).